*metals*

MDPI

*Article*

# Characterization of EAF and LF Slags Through an Upgraded Stationary Flowsheet Model of the Electric Steelmaking Route

**Ismael Matino [1,*], Alice Petrucciani [1], Antonella Zaccara [1,2], Valentina Colla [1], Maria Ferrer Prieto [3] and Raquel Arias Pérez [3]**

[1] TeCIP Institute, Scuola Superiore Sant'Anna, Via Moruzzi 1, 56124 Pisa, Italy; alice.petrucciani@santannapisa.it (A.P.); antonella.zaccara@santannapisa.it (A.Z.); valentina.colla@santannapisa.it (V.C.)
[2] Dipartimento di Ingegneria Industriale, Università di Padova, Via Gradenigo, 6/a, 35131 Padova, Italy
[3] Sidenor Investigacion Y Desarrollosa, Barrio Ugarte, 48970 Basauri, Spain; maria.ferrer@sidenor.com (M.F.P.); raquel.arias@sidenor.com (R.A.P.)
* Correspondence: ismael.matino@santannapisa.it; Tel.: +39-3931523444

**Abstract:** The current, continuous increase in attention toward preservation of the environment and natural resources is forcing resource-intensive industries like steelworks to investigate new solutions to improve resource efficiency and promote the growth of a circular economy. In this context, electric steelworks, which inherently implement circularity principles, are spending efforts to enhance valorization of their main by-product, namely slags. A reliable characterization of the slag's composition is crucial for the identification of the best valorization pathway, but, currently, slag monitoring is often discontinuous. Furthermore, in the current period of transformation of steel production, preliminary knowledge of the effect of modifications of operating practices on slags composition is crucial to assessing the viability of these modifications. In this paper, a stationary flowsheet model of the electric steelmaking route is presented; this model enables joint monitoring of key variables related to process, steel and slags. For the estimation of the content of most compounds in slags, the average relative percentage error is below 20% for most of the considered steel families. Thus, the tool can be considered suitable for scenario analyses supporting slag valorization. Higher performance is achievable by exploiting more reliable data for model tuning. These data can be obtained via novel devices that gather more numerous and representative data on the amount and composition of slags.

**Keywords:** electric steelmaking; slags; slags composition; modelling and simulation; by-products valorization



Academic Editor: Chenguang Bai

Received: 31 January 2025
Revised: 26 February 2025
Accepted: 28 February 2025
Published: 4 March 2025

**Citation:** Matino, I.; Petrucciani, A.; Zaccara, A.; Colla, V.; Prieto, M.F.; Pérez, R.A. Characterization of EAF and LF Slags Through an Upgraded Stationary Flowsheet Model of the Electric Steelmaking Route. *Metals* **2025**, *15*, 279. https://doi.org/10.3390/met15030279



## 1. Introduction

Steelmaking is pivotal to achieving the ambitious targets of decarbonization and climate neutrality set by the European Union in its European Green Deal, which aims to make Europe a leader in sustainability and the first climate-neutral continent [1]. Furthermore, the steel sector is also at the center of the transition to a circular economy promoted by the European New Circular Economy Action Plan [2], which aims to make Europe cleaner and more competitive. Steel is indeed a permanent, durable and 100% recyclable and reusable material, and the electric-scrap-based production route implements a circular economy practice since its origins [3].

Steel industries are highly committed to improving and modifying their technologies, targeting C-footprint reduction [4,5] by applying new production routes [6], optimizing the

processes from the energetic point of view [7–9], promoting environmental-friendly scrap treatment solutions [10], and substituting fossil materials [11–13]. Furthermore, significant attention is paid to resource efficiency, by-products valorization practices (internal by recycling and external by reuse) [14,15] and promotion of industrial symbiosis solutions [16] involving by-products such as slag, sludges, mill scales, dusts, water and off-gases. In particular, slags represent 90% in mass of all by-products generated by steel production [17,18] and are valuable sources of secondary raw materials that are used in several industrial sectors through industrial symbiosis; these solutions also reduce issues concerning the slags' disposal [19–22].

However, slag composition is often analyzed in a discontinuous way, as the industrial focus is on the main product (i.e., steel) and standard analytical procedures for both liquid and solid slags are lengthy and quite cumbersome. Moreover, in the current period of transformation of steel production processes, preliminary knowledge of the effect on slags of changes of operating practices, conditions or raw materials is crucial to assessing the viability of these changes and to adjusting the whole value chain accordingly. Therefore, a strong demand is emerging for new sensing devices and characterization methods for liquid and solid slags that will enable fast and sufficiently accurate assessment of their chemical and physical properties. Several publications are available on this topic in the literature. For instance, novel and different types of analytical methods were investigated by Herbelin et al. [23] and Menad et al. [24]. Different works have investigated the use of laser-induced breakdown spectroscopy (LIBS) for rapid and real-time analysis of slag chemistry [25,26], also coupling it with Machine Learning (ML) techniques [27].

Furthermore, the development of tools to estimate steel slag composition in current and future process configurations/operating conditions is fundamental. These tools can be used to monitor slag and possibly support the modification of the steelmaking process to optimize slag features by preserving steel quality while decreasing environmental impact; such tools could also drive the selection of the best valorization pathway for slag. Following this demand, some models can be found in the literature that aim to estimate features of steel slag. Different approaches are addressed in [28] for the characterization of electric arc furnace (EAF) slag, but issues were encountered because of unreliable data and the complexity of the EAF process, and this highlights the necessity of using a good dataset for model development. Hay et al. propose an improved EAF process model that allows, among other outcomes, the computation of EAF slag chemistry [29]. Similarly, Fathi et al. describe in [30] an improved version of a complex model developed by Logar et al. [31,32] to simulate the EAF process and compute, among other outputs, also some slag features through the dedicated chemical and slag module. A kinetic model was developed by Harada et al. to predict changes in chemical composition in molten steel, slag and inclusions in the ladle refining stage [33,34], and explain the mechanism underlying the change in the chemical composition of inclusion. The results in terms of molten steel and slag composition correspond to operational data.

Although all these models are valuable, some of them simulate only one slag type or only some areas/steps of steelmaking [29]. Some models are too complex to be simply customized/validated with data that are available in standard industrial practice, integrated with new streams and units and/or used by process operators [30–34]. Furthermore, their results are affected by data unreliability [28]. All these aspects represent important limitations to the use of these tools within investigations concerning slag composition, as they can hamper a global vision of process, product and by-products.

The present paper describes the use of an Aspen Plus®-based stationary flowsheet model of the electric steelmaking route that provides an estimate of EAF and Ladle Furnace (LF) slags compositions. The model was tuned and upgraded with respect to a previous

version using a significant amount of process data (more than one thousand heats data) provided by a Spanish steelworks and concerning, among other information, the amount and composition of slags. Compared to existing state-of-the-art simulation tools, this model is intended to be easily tuned and customized by exploiting data that are commonly available in the industrial files without the need to take any new measurements for this purpose, and is intended to estimate variables that are normally monitored in the standard industrial operating practice, such as steel amount and composition, slags amount and composition (although in real practice, this last measurement is done often discontinuously), energy consumption, temperatures and $CO_2$ emissions. This model can be easily used by process operators thanks to the possibility of ad hoc customization of a graphic user interface. Furthermore, thanks to its modular structure, the model allows the integration of further units/streams to investigate the effects of process modifications on slags. Specifically, the model will enable studies related to the foreseen evolution of the electric steelmaking route towards novel practices that enhance the environmental sustainability of steel production. Such practices include the use of direct reduced iron (DRI) as a partial replacement for scrap, replacement of fossil C-bearing materials with biochar or other renewable C sources (e.g., plastics), and the use of blends of natural gas and hydrogen as fuel for the burners. By jointly considering the composition of steel and slags together with other key process variables, this model can be used to estimate slags composition for a specific steel production in the context of standard or novel process configurations/operating conditions. It can also be used to assess the viability of solutions to synergistically improve steel quality and slag composition and increase the economic and environmental sustainability of the production process.

## 2. Materials and Methods

### *2.1. Brief Description of the Initial Version of the Model*

The present work was carried out using as a basis an EAF steelmaking stationary flowsheet process model developed in the Aspen Plus® V8.4 environment within the project entitled "*Environmental impact evaluation and effective management of resources in the EAF steelmaking—EIRES*" [35,36]. That model represented the whole electric steelmaking route until the beginning of continuous casting (CC) and was focused on the assessment of the environmental impact of common and uncommon process practices [37,38]. Several Aspen Plus® internal unit blocks (e.g., reactors, heaters, mixers, separators) were combined with ad-hoc calculators and design specification units to reproduce the various phenomena involved (e.g., melting, oxidation, tapping, refining, degassing, heat exchange) in the different process steps. The model is composed of six main consecutive areas: 1. charge and melting; 2. additions to the EAF and the EAF process, slag formation, deslagging and tapping; 3. transportation of the ladle; 4. LF treatment; 5. vacuum degassing (VD) treatment (if required) and the final stages of secondary metallurgy; and 6. the receipt of steel in tundish and the beginning of CC. The combination of the previously mentioned units allows for the consideration of different phenomena as a sum of effects in terms of mass and energy flows, chemical and physical balances, reactions and thermodynamic equilibria and transformations based on the literature, but especially on industrial data and experience. Besides equilibrium between different phases and reactions that are automatically considered by the software, the main reactions that were included in the initial version of the model are listed below, specifying their type, the main processes in which they are involved and the main unit operations in which they mainly occur.

$2C + O_2 \rightarrow 2CO$ Oxidation related to decarburization (EAF mainly, LF) and to the deoxidation process (VD) (1)

$C + O_2 \rightarrow CO_2$ Oxidation related to decarburization (EAF mainly, LF) (2)

$$2CO + O_2 \rightarrow 2CO_2 \quad \text{Oxidation related to post-combustion of CO (EAF, LF)} \tag{3}$$

$$2CO \leftarrow\rightarrow CO_2 + C \quad \text{Boudouard equilibrium (EAF, LF)} \tag{4}$$

$$2Fe + O_2 \rightarrow 2FeO \quad \text{Oxidation related to scrap components (EAF), to the deoxidation process (EAF, LF mainly) and to alloying additions (LF)} \tag{5}$$

$$Si + O_2 \rightarrow SiO_2 \quad \text{Oxidation related to scrap components (EAF), to the deoxidation process (EAF, LF mainly) and to alloying additions (LF)} \tag{6}$$

$$4Al + 3O_2 \rightarrow 2Al_2O_3 \quad \text{Oxidation related to the deoxidation process (EAF, LF mainly), to fluxes additions and slag formation (EAF, LF) and to alloying additions (LF)} \tag{7}$$

$$FeO + C \rightarrow Fe + CO \quad \text{Reduction related to decarburization (EAF)} \tag{8}$$

$$Ti + O_2 \rightarrow TiO_2 \quad \text{Oxidation related to scrap components (EAF) and to alloying additions (LF)} \tag{9}$$

The model was developed to be tuned and adapted to different steelworks and then exploited using only information related to process parameters and variables that are usually used/collected/monitored in standard industrial operating practice. The following information is required for model customization, tuning and use: scraps amount and type, amount of other metallic (e.g., pig iron) and non-metallic standard charge material, desired temperature during the different process steps, amounts of used fuels, flowrates of injected compounds, amount of Fe alloys or of further additions and pressure during VD. On the other hand, the following information is required only in the tuning and validation stage: amount and composition of steel, by-products and further output streams and amount of required energy. Generally, for the previously listed variables and parameters, data are available on a heat basis. In cases where there is a lack of industrial data, data from the literature can be used.

The model was conceived such that its outputs can be easily interpreted by industrial operators thanks to the option to link it with a graphical user interface including ad hoc customized Microsoft Excel® sheets. More information on the first version of the model can be found in [35,36].

When the model was first developed, applications of industry 4.0 concepts were not yet widespread in the steel sector, and data collection and extraction were not as established as they are now. Therefore, although the model showed good performance in terms of steel composition and energy distribution, assessment of the performance as far as slag composition is concerned was not possible due to the slag analyses being highly discontinuous, which prevents an extensive comparison of real and simulated data. Therefore, several simplifying assumptions were made during model development due to lack of industrial data on this aspect.

### *2.2. Upgraded Model*

The model overviewed in Section 2.1 has been improved over the years thanks to the increased availability of data from industries and to a growing industrial interest in this kind of tool. The model was updated in the Aspen Plus® V11 environment. Figure 1 depicts all the different sections of the model and related main inputs and outputs.

In particular, the availability of several data belonging to more than 1500 heats produced by a Spanish electric steelworks made it possible to upgrade the model by specifically improving the parts related to the calculation of slag composition. The available industrial data were collected under standard operating conditions (revamping periods were avoided) on a heat basis and do not encompass dynamic information on the process. They include information on charges and related composition (e.g., average composition of used scraps), operating conditions, additions (i.e., Fe-alloys and non-metal additions) and related com-

position, liquid metal amount and composition along the process, and EAF and LF slags compositions. These data refer to the production of several steel grades that were grouped in eight steel families: Alloyed Case Hardening (ACH), Alloyed Quenched & Tempered (AQT), Bearing (BEAR), Carbon Case Hardening (CCH), Free-Cutting (FC), Microalloyed (MA) and Spring (SPR).

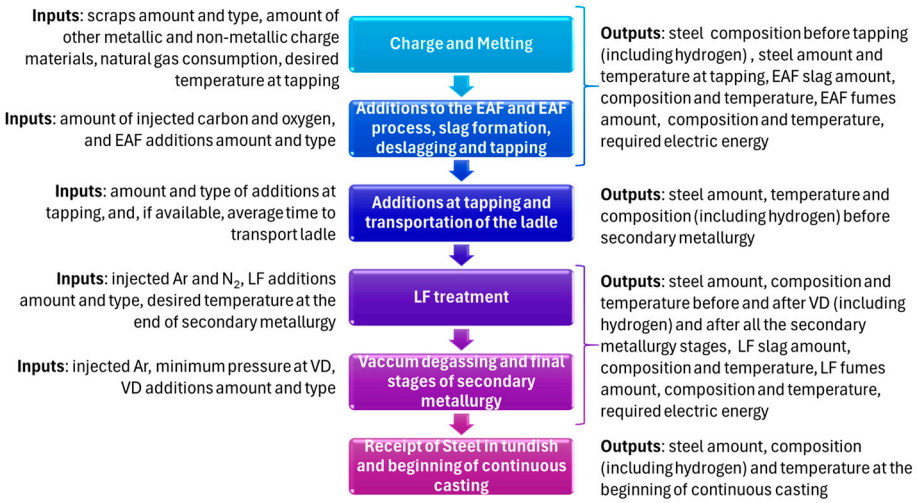


**Figure 1.** Main sections, inputs and outputs of upgraded model.

After a preliminary stage of outliers removal to eliminate unreliable measurements, the industrial data were clustered according to the steel families, the production steps and/or the measurement points. Simple statistical analyses were carried out to obtain useful information for model improvement and for related tuning based on the different steel families.

Starting from the charge and melting section of the model, compared to the previous model version, more scrap types (14 instead of 3) are considered in the upgraded model. The mass fraction of main chemical components apart from C and Fe are reported in Table 1.

**Table 1.** Content of main chemical components of considered scraps.

| | Mn | P | S | Cu | Cr | Ni | Mo | Sn |
|---|---|---|---|---|---|---|---|---|
| **Scrap ID** | | | | *w/w* | | | | |
| S1 | - | 0.0100 | 0.0250 | 0.0400 | 0.0350 | 0.0350 | 0.0200 | 0.0050 |
| S2 | 0.0860 | 0.0004 | 0.0350 | 0.1400 | 0.0920 | 0.2720 | 0.0760 | 0.0090 |
| S3 | 0.1030 | 0.0070 | 0.0300 | 0.1850 | 0.1300 | 0.2010 | 0.0650 | 0.0090 |
| S4 | - | 0.0250 | 0.0400 | 0.3400 | 0.0700 | 0.1000 | 0.0250 | 0.0200 |
| S5 | 0.0790 | 0.0230 | 0.0560 | 0.3900 | 0.1000 | 0.1070 | 0.0200 | 0.0140 |
| S6 | 0.1440 | 0.0090 | 0.0310 | 0.2780 | 0.0920 | 0.1140 | 0.0310 | 0.0130 |
| S7 | - | 0.0150 | 0.0400 | 0.1700 | 0.0600 | 0.0700 | 0.0200 | 0.0130 |
| S8 | 0.0630 | 0.0020 | 0.0070 | 0.0490 | 0.0140 | 0.0320 | 0.0070 | 0.0070 |
| S9 | 0.0630 | 0.0040 | 0.0140 | 0.1030 | 0.0270 | 0.0590 | 0.0120 | 0.0070 |
| S10 | 0.1240 | 0.0080 | 0.0330 | 0.1980 | 0.1450 | 0.2260 | 0.0690 | 0.0100 |
| S11 | 0.1130 | 0.0050 | 0.0230 | 0.2030 | 0.2050 | 0.3120 | 0.1620 | 0.0100 |
| S12 | 0.1170 | 0.0050 | 0.0190 | 0.1960 | 0.2260 | 0.5660 | 0.1820 | 0.0100 |
| S13 | 0.0810 | 0.0080 | 0.0200 | 0.1060 | 0.0640 | 0.0890 | 0.0330 | 0.0070 |
| S14 | 0.0890 | 0.0150 | 0.0570 | 0.2750 | 0.1270 | 0.2610 | 0.0690 | 0.0130 |

The scraps are charged together with dolomitic lime in solid form; the charging was simplified and carried out in a single stage, since it does not affect the operation of this

kind of model. The charge is melted by exploiting multiple energy sources: electrical energy, combustion of methane and chemical energy from further fossil sources (e.g., coke) and exothermic reactions. The model computes the electrical energy required to melt the scrap, taking into account the energy balance, the enthalpies involved and the desired temperature at tapping, and considering the following equation to estimate the liquidus temperature ($T_{liquidus}$ in K):

$$T_{liquidus} = 1811\text{K} - (83 \cdot \%C + 9 \cdot \%Si + 2 \cdot \%Mn + 5 \cdot \%Ni + 1 \cdot \%Cr + 5 \cdot \%Mo + 40 \cdot \%S + 72 \cdot \%N) \quad (10)$$

where $\%C$, $\%Si$, $\%Mn$, $\%Ni$, $\%Cr$, $\%Mo$, $\%S$ and $\%N$ are the weight percentages of the listed elements in the charge mix.

Together with scrap melting, hydrogen formation from the splitting of atmospheric moisture and its dissolution in the molten bath is simulated via water-splitting reaction, as follows:

$$2H_2O \rightarrow 2H_2 + O_2 \quad (11)$$

After the melting, in section 2 of the model, additions to EAF are simulated by feeding carbon (mainly used for the formation of the foamy slag), a series of scorifying materials and deoxidizing agents, as well as further materials (if required). A dedicated "hierarchy block" was used in the model for the additions. For simplification reasons, it includes all possible substances in terms of Fe-alloys and metals, and non-metallic materials (although some of them are used only in some process steps), and it is replicated in each "addition point" of the process.

With respect to the original model version, an estimate of carbon released by electrodes was included using empirical equations. Furthermore, while in the first version of the model, only a few reactions were included (see Equations (1)–(9) in Section 2.1) due to a lack of information, in the upgraded model, several further reactions are considered, and these are listed below. To avoid list duplication, it includes reactions occurring in EAF and LF; therefore, the list specifies their type, the processes in which they are involved, and the main unit operations in which they mainly occur. Operating conditions affect reaction occurrence. It is worth mentioning that some reactions are missing, while other ones are simplified: only aspects that can be validated with available data or with data commonly available in steelworks are included in the model. Furthermore, simplifications were included to limit the model's complexity and computational burden and avoid convergence issues.

$2Ca + O_2 \rightarrow 2CaO$ Oxidation related to fluxes additions and slag formation (EAF, LF) and to the deoxidation process (EAF, LF mainly) (12)

$2Mg + O_2 \rightarrow 2MgO$ Oxidation related to fluxes additions and slag formation (EAF, LF) (13)

$4Cr + 3O_2 \rightarrow 2Cr_2O_3$ Oxidation related to scrap components (EAF) and to alloying additions (LF) (14)

$2W + 3O_2 \rightarrow 2WO_3$ Oxidation related to scrap components (EAF) and to alloying additions (LF) (15)

$2Mo + 3O_2 \rightarrow 2MoO_3$ Oxidation related to scrap components (EAF) and to alloying additions (LF) (16)

$4B + 3O_2 \rightarrow 2B_2O_3$ Oxidation related to scrap components (EAF) and to alloying additions (LF) (17)

$4V + 5O_2 \rightarrow 2V_2O_5$ Oxidation related to scrap components (EAF) and to alloying additions (LF) (18)

$2Ni + O_2 \rightarrow 2NiO$ Oxidation related to scrap components (EAF) and to alloying additions (LF). It occurs only under strong oxidizing conditions (19)

$2Co + O_2 \rightarrow 2CoO$ Oxidation related to scrap components (EAF) and to alloying additions (LF). It occurs only under strong oxidizing conditions (20)

$2Pb + O_2 \rightarrow 2PbO$ Oxidation related to scrap components (Pb is lost during fumes formation where in the presence of oxygen oxidize) and to alloying additions (LF) (21)

$2Mn + O_2 \rightarrow 2MnO$ Oxidation related to scrap components (EAF), to the deoxidation process (EAF, LF mainly) and to alloying additions (LF) (22)

$4P + 5O_2 \rightarrow 2P_2O_5$ Oxidation reaction related to scrap components (EAF) and the dephosphorization process (EAF mainly, LF) (23)

$2Zn + O_2 \rightarrow 2ZnO$ Oxidation related to scrap components and EAF dust formation (EAF) (24)

$S + CaO \rightarrow CaS + O$ Desulphuration related to fluxes additions (EAF, LF mainly) (25)

$3\,CaO + 2\,Al + 3S \rightarrow 3\,CaS + Al_2O_3$ Desulphuration related to fluxes additions (EAF, LF mainly) (26)

$S + O_2 \rightarrow SO_2$ Oxidation (EAF) (27)

$2S + 3O_2 \rightarrow 2SO_3$ Oxidation (EAF) (28)

$2SO_2 + O_2 \rightarrow 2SO_3$ Oxidation (EAF) (29)

$2N + O_2 \rightarrow 2NO$ Oxidation (EAF) (30)

$N + O_2 \rightarrow NO_2$ Oxidation (EAF) (31)

$2NO + O_2 \rightarrow 2NO_2$ Oxidation (EAF) (32)

$2H_2 + O_2 \rightarrow H_2O$ Oxidation (EAF) (33)

The progresses of the reactions were simulated in different kinds of reactor blocks, as reaction equilibrium constants, reaction yields, or kinetic factors are used and calibrated based on the reaction type and on the available information. Some of these parameters are empirical or are obtained from the analyses of the industrial data, while other ones are found in the literature or directly in the software database.

For instance, the yield parameter related to the dephosphorization reaction (23) is calibrated by implementing a correlation obtained from literature data [39] that represents the dependence of phosphorous partition (expressed as mass fraction) between slag ($(P_2O_5)$) and liquid metal ($[P]$) on the basicity index ($IB_1$). As follows:

$$(P_2O_5)/[P] = 27.22 \cdot IB_1 - 10.60 + j \quad (34)$$

where $j$ is an adjustment empirical factor and $IB_1$ is expressed as follows:

$$IB_1 = (CaO_{w/w})/(SiO_{2w/w} + Al_2O_{3w/w}) \quad (35)$$

where $CaO_{w/w}$, $SiO_{2w/w}$ and $Al_2O_{3w/w}$ are the mass fractions of the respective compounds in the slag.

At this stage of the process, sulfur partition (expressed as mass fraction) equilibria between slag ($(S)$) and metal ($[S]$) are also evaluated in the upgraded model thanks to the configuration of dedicated calculator blocks that control some auxiliary units. The calculator blocks estimate the distribution of sulfur between slag and molten metal by making interpolations/extrapolations of three functions representing the sulfur metal−slag partition ratios as a function of the oxidation conditions of the system (represented by the FeO weight percentage in the slag $(\%FeO)$) for different basicity values ($IB_2$) and for a

temperature around 1600 °C. The functions are reported below and reproduce the three theoretical curves that can be found in [40], as follows:

$$\frac{(S)}{[S]} = \begin{cases} \frac{2.51 \cdot 10^{-1}}{1.65 \cdot 10^{-3} \cdot \%FeO^3 - 4.33 \cdot 10^{-2} \cdot \%FeO^2 + 3.23 \cdot 10^{-1} \cdot \%FeO + 2.43 \cdot 10^{-4}}, \ IB_2 = 1.5 \\ \frac{5.55 \cdot 10^{-1} \cdot \%FeO^{-1}}{-3.43 \cdot 10^{-3} \cdot \ln(\%FeO) + 1.20 \cdot 10^{-1}} + 6.67 \cdot 10^{-1}, IB_2 = 2 \\ \frac{-18.15 \cdot \%FeO^{-1}}{-3.14 \cdot 10^{-1} \cdot \ln(\%FeO) + 3.59} + 7.12, \ IB_2 = 4 \end{cases} \quad (36)$$

where $IB_2$ is computed as follows:

$$IB_2 = (CaO_{w/w} + MgO_{w/w})/(SiO_{2w/w} + Al_2O_{3w/w}) \quad (37)$$

and $CaO_{w/w}$, $MgO_{w/w}$, $SiO_{2w/w}$ and $Al_2O_{3w/w}$ are the mass fractions of the respective compounds in the slag.

All contributions in terms of heat generation (exothermic reactions) or heat removal (melting of solid inputs or endothermic reactions) are estimated by direct calculations performed by the software using its internal database or by computing blocks that were added ad hoc.

Although in real operations, the EAF slag formed is removed from the molten bath in a single tapping step, in the model, various removal steps are carried out and then mixed to simplify the simulation structure. A special block was inserted in this version of the model to estimate the amount of slag dragged during the tapping stage. It was configured taking into account the range of variability of dragged slag by considering available data related to the number of pixels representing slag in a picture of tapped liquid metal.

The fumes generated at these process stages are also separated from the molten bath using various "flash" units that carry out liquid/vapor equilibrium calculations. However, a lack of continuous and numerous data hampers the validation of the estimates of the amount and composition of fumes provided by the model.

During tapping, additions are made to the melt to start the secondary metallurgy processes and the elaboration concerning secondary metallurgy slag. These additions and the related heat losses due to their melting were considered in the upgraded model in a new dedicated part of model section 3.

In model section 4, LF is simulated: Ar and $N_2$ are injected, deoxidation reactions (e.g., reactions (6) (7) (12) (22)) occur by the addition of deoxidant agents to minimize the oxygen content, desulphurization takes place (reactions (25) and (26)) and there is some refining of dephosphorization (reaction (23)). In an approach similar to that used in the EAF section, the reaction parameters are tuned with available data belonging to this part of the process. Alloys are also added to the ladle and the sulfur partition is computed, both in the same way as described for EAF. The heat is provided at this stage with electrical energy, which is computed by the model through a design specification block whose purpose is to ensure the desired temperature is attained at the end of secondary metallurgy. For this calculation, energy balances and involved enthalpies are considered.

VD is the process step considered by model section 5. The main unit in this section is a "flash" unit, where pressure is lowered to the desired value and, consequently, gaseous compounds are separated according to liquid/vapor equilibrium. In the upgraded version of the model, the influence of argon injection on the removal of hydrogen and nitrogen are considered through some additional blocks complementary to the flash unit. In particular, a calculator block was customized with a series of functions reproducing the curves reported in [41] and for interpolation/extrapolation computations. These functions are reported below:

$$H_{2out} = \begin{cases} 7.58 \cdot 10^{-10} \cdot Ar_{in}{}^{6} - 6.78 \cdot 10^{-8} \cdot Ar_{in}{}^{5} + 2.55 \cdot 10^{-6} \cdot Ar_{in}{}^{4} - 1.18 \cdot 10^{-4} \cdot Ar_{in}{}^{3} + 6.34 \cdot 10^{-3} \cdot Ar_{in}{}^{2} - 1.97 \cdot 10^{-1} \cdot Ar_{in} + 2.85, & H_{2in} = 2.8 \text{ ppm} \\ 1.05 \cdot 10^{-8} \cdot Ar_{in}{}^{6} - 1.38 \cdot 10^{-6} \cdot Ar_{in}{}^{5} + 7.40 \cdot 10^{-5} \cdot Ar_{in}{}^{4} - 2.13 \cdot 10^{-3} \cdot Ar_{in}{}^{3} + 3.90 \cdot 10^{-2} \cdot Ar_{in}{}^{2} - 5.20 \cdot 10^{-1} \cdot Ar_{in} + 4.71, & H_{2in} = 4.7 \text{ ppm} \\ 2.46 \cdot 10^{-8} \cdot Ar_{in}{}^{6} - 3.46 \cdot 10^{-6} \cdot Ar_{in}{}^{5} + 1.96 \cdot 10^{-4} \cdot Ar_{in}{}^{4} - 5.77 \cdot 10^{-3} \cdot Ar_{in}{}^{3} + 9.64 \cdot 10^{-2} \cdot Ar_{in}{}^{2} - 9.86 \cdot 10^{-1} \cdot Ar_{in} + 6.55, & H_{2in} = 6.7 \text{ ppm} \end{cases} \quad (38)$$

$$N_{2out} = \begin{cases} 5.26 \cdot 10^{-9} \cdot Ar_{in}{}^{6} - 5.44 \cdot 10^{-7} \cdot Ar_{in}{}^{5} + 1.74 \cdot 10^{-5} \cdot Ar_{in}{}^{4} - 1.81 \cdot 10^{-4} \cdot Ar_{in}{}^{3} + 5.96 \cdot 10^{-3} \cdot Ar_{in}{}^{2} - 3.67 \cdot 10^{-1} \cdot Ar_{in} + 21.02, & N_{2in} = 20 \text{ ppm} \\ -6.79 \cdot 10^{-9} \cdot Ar_{in}{}^{6} + 9.70 \cdot 10^{-7} \cdot Ar_{in}{}^{5} - 5.14 \cdot 10^{-5} \cdot Ar_{in}{}^{4} + 1.19 \cdot 10^{-3} \cdot Ar_{in}{}^{3} - 5.17 \cdot 10^{-3} \cdot Ar_{in}{}^{2} - 5.11 \cdot 10^{-1} \cdot Ar_{in} + 30.56, & N_{2in} = 30 \text{ ppm} \\ 2.39 \cdot 10^{-8} \cdot Ar_{in}{}^{6} - 2.67 \cdot 10^{-6} \cdot Ar_{in}{}^{5} + 1.16 \cdot 10^{-4} \cdot Ar_{in}{}^{4} - 2.80 \cdot 10^{-3} \cdot Ar_{in}{}^{3} + 5.49 \cdot 10^{-2} \cdot Ar_{in}{}^{2} - 1.21 \cdot Ar_{in} + 40.35, & N_{2in} = 40 \text{ ppm} \\ 1.77 \cdot 10^{-8} \cdot Ar_{in}{}^{6} - 2.03 \cdot 10^{-6} \cdot Ar_{in}{}^{5} + 9.07 \cdot 10^{-5} \cdot Ar_{in}{}^{4} - 2.16 \cdot 10^{-3} \cdot Ar_{in}{}^{3} + 4.71 \cdot 10^{-2} \cdot Ar_{in}{}^{2} - 1.46 \cdot Ar_{in} + 49.79, & N_{2in} = 50 \text{ ppm} \\ 1.74 \cdot 10^{-8} \cdot Ar_{in}{}^{6} - 1.32 \cdot 10^{-6} \cdot Ar_{in}{}^{5} + 1.10 \cdot 10^{-5} \cdot Ar_{in}{}^{4} + 9.09 \cdot 10^{-4} \cdot Ar_{in}{}^{3} + 6.25 \cdot 10^{-3} \cdot Ar_{in}{}^{2} - 1.61 \cdot Ar_{in} + 59.08, & N_{2in} = 60 \text{ ppm} \\ 2.65 \cdot 10^{-8} \cdot Ar_{in}{}^{6} - 2.34 \cdot 10^{-6} \cdot Ar_{in}{}^{5} + 5.94 \cdot 10^{-5} \cdot Ar_{in}{}^{4} - 5.34 \cdot 10^{-4} \cdot Ar_{in}{}^{3} + 3.91 \cdot 10^{-3} \cdot Ar_{in}{}^{2} - 2.21 \cdot Ar_{in} + 68.46, & N_{2in} = 70 \text{ ppm} \\ 6.68 \cdot 10^{-8} \cdot Ar_{in}{}^{6} - 8.54 \cdot 10^{-6} \cdot Ar_{in}{}^{5} + 4.44 \cdot 10^{-4} \cdot Ar_{in}{}^{4} + 1.26 \cdot 10^{-2} \cdot Ar_{in}{}^{3} - 2.38 \cdot 10^{-1} \cdot Ar_{in}{}^{2} - 3.99 \cdot Ar_{in} + 79.73, & N_{2in} = 80 \text{ ppm} \end{cases} \quad (39)$$

where $H_{2out}$ and $N_{2out}$ are, respectively, hydrogen and nitrogen in steel after VD, expressed in ppm; $H_{2in}$ and $N_{2in}$ are, respectively, hydrogen and nitrogen in the steel before VD and $Ar_{in}$ is the volume of insufflated argon, expressed in $m^3$.

Eventually, additional corrections to the hydrogen content in the steel are made by considering further calculations based on its solubility in liquid steel ($H_{2sol}$ in ppm) according to Sieverts' law [42], which, for the liquid state, was reproduced through the following relationship as a function of the temperature (T in °C):

$$H_{2sol} = 2.8 \cdot 10^{-2} \, T - 18.59 \quad (40)$$

This relationship is used to check the hydrogen content in the liquid steel on the whole simulated route.

During VD, additions can be made to the ladle in small amounts, and these are represented in the model through a dedicated hierarchy block as described before for the EAF.

After the simulation of all the secondary metallurgy steps, slag is separated from the liquid steel. In the real process, LF slag remains suspended on the steel, which is removed from the bottom of the ladle, while the ladle holding the remaining LF slag is taken to a different area, where the slag is poured into the LF slag pot. In the model, for the sake of simplification and better management, the LF slag is separated through various steps and then mixed in a single stream.

The last model section refers to the receipt of steel to the tundish and the start of continuous casting. A simple heat-exchanger unit is used to simulate the steel cooling.

In the whole model, some adjustment parameters are included to compensate, whenever possible, for uncertainties in the data or for the lack of complete information.

## 3. Results

After the tuning, which was carried out using 70% of the available industrial dataset (about 950 heats data), the upgraded model was used and tested to simulate a multitude of heats of the eight considered steel families; the test dataset corresponds to 30% of the available industrial dataset (about 450 heats data). In the test phase, the model was validated by comparing its outcomes to real industrial data included in the test dataset. Simulations generally need from a few minutes to a maximum of 15 min to converge; thus, the model can be considered a quite fast tool for scenario analyses.

Real data concerning slag composition were compared to the results of the test simulations, and relative percentage error was computed as follows:

$$RPE = 100 \cdot | (X_{real} - Y_{sim}) / X_{real} | \quad (41)$$

Figures 2 and 3 provide Pareto diagrams showing the amount of tested heats giving a specified range of RPE for the components constituting on average more than 95% of EAF (Figure 2) and LF (Figure 3) slags mass.

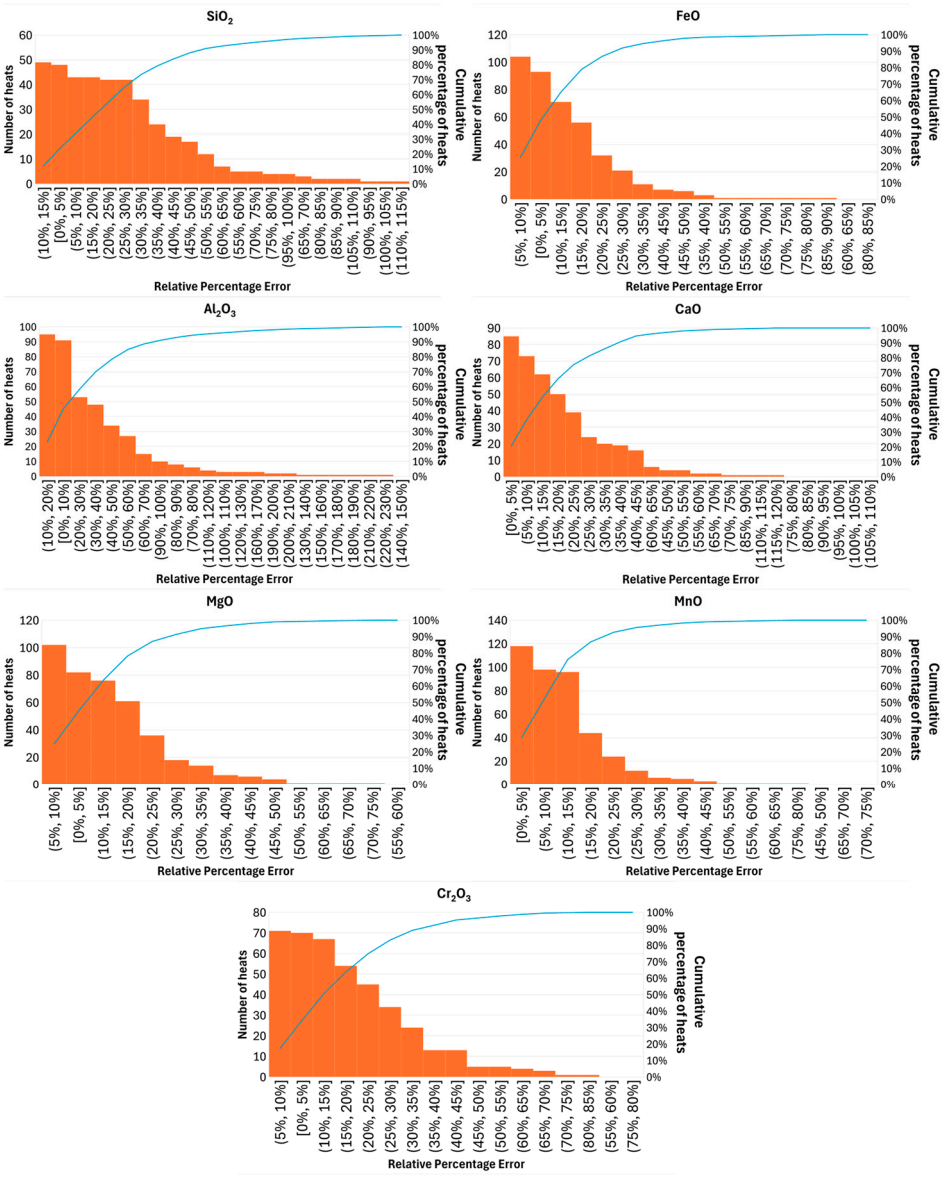


**Figure 2.** Pareto diagrams of RPEs of tested heats for the content of main EAF slag compounds.

In addition, as an example, Figure 4 shows RPEs for the main compounds of EAF and LF slags belonging to a single simulated heat.

All figures show that the model is capable of suitably estimating the content (i.e., mass fraction) of different slag compounds, although with different levels of accuracy. Indeed, more than 70% of tested heats give RPEs as follows:

- lower than 25% in the case of FeO, CaO, MgO, MnO and $Cr_2O_3$ for EAF slag and of $SiO_2$ and CaO for LF slag;
- lower than 40% in the case of $SiO_2$ and $Al_2O_3$ for EAF slag and of $Al_2O_3$ for LF slag;
- lower than 50% in the case of MgO for LF slag.

This is underlined by computing further accuracy indexes, namely Mean Relative Percentage Errors (MRPE), Root Mean Squared Error (RMSE) and Scatter Index (SI), for each simulated steel family and for each considered slag compound, which are defined as follows:

$$\mathrm{MRPE} = 100 \cdot (1/n)\, \Sigma\, |\, (X_{real} - Y_{sim})/X_{real}\, | \tag{42}$$

$$\mathrm{RMSE} = [1/n \cdot \Sigma\, (X_{real} - Y_{sim})^2]^{0.5} \tag{43}$$

$$SI = 100 \cdot RMSE / [1/n \cdot \Sigma (X_{real})] \quad (44)$$

where $n$ is the number of samples, $X_{real}$ is the real observed value and $Y_{sim}$ is the simulated value. The values of the obtained accuracy indexes are reported in Table 2 for EAF slag and Table 3 for LF slag. In order to fully assess the model performances, the Percentage Deviation Coefficient (PVC) of each variable in the test dataset is also provided and it is defined as the percentage ratio of the standard deviation over the mean value.

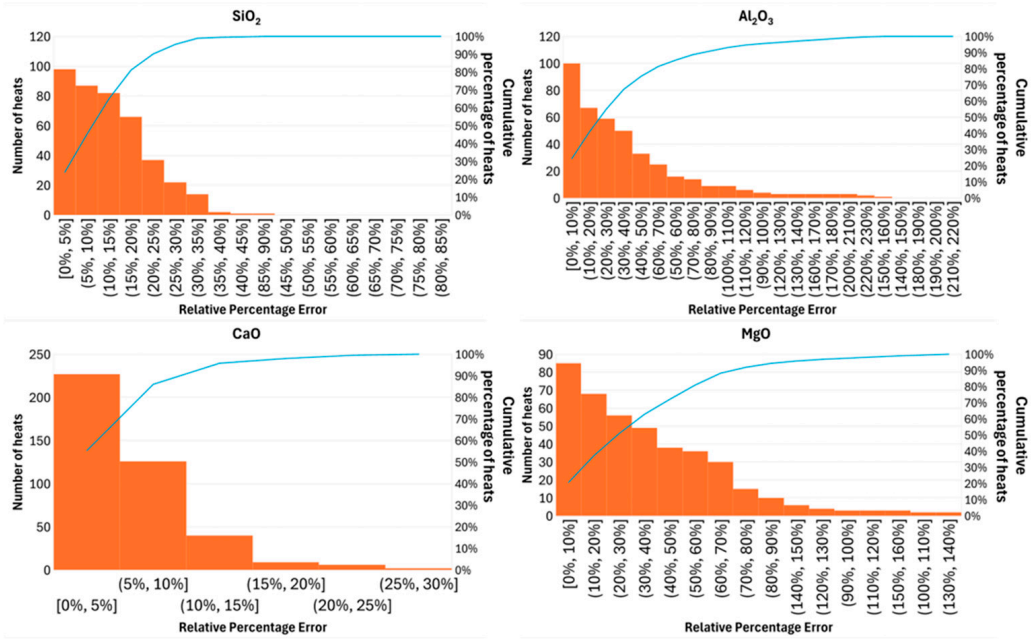


**Figure 3.** Pareto diagrams of RPEs of tested heats for the content of main LF slag compounds.

For EAF slag, the best accuracies are obtained in the estimates of the contents of FeO, CaO, MgO and MnO; in these cases, the MRPE is lower than 20% for seven of the eight families. Also, the content of $Cr_2O_3$ is generally predicted well, with MRPE values lower than 19%, apart from two families (i.e., ACH, BEAR). The worst accuracy is observed in the estimate of the content of $Al_2O_3$, as the related values of MRPE are lower than 40% for all steel families apart from AQT and CCH. Finally, the MRPE values observed for the content of $SiO_2$ are lower than 31% for all steel families. These accuracy values are in line with what is shown by Figure 2.

Issues in the estimate of the content of $Al_2O_3$ (MRPE < 36% apart for CQT and SPR steel families) are evident also for LF slag, in which also the estimate of the content of MgO has MRPE values lower than 26% for only five steel families (i.e., ACH, BEAR, CCH, FC, MA). These aspects are in line with what is reported in Figure 3. The best results are observed for the estimates of the contents of CaO and $SiO_2$, for which generally MRPE values lower than 9% and 15%, respectively, are observed; the only exception is for the BEAR steel family.

Generally, higher errors are observed for steel families including more numerous steel grades (e.g., CQT), which show a higher variability in slags composition, or for steel families for which fewer data are available because related steel grades are less frequently produced (e.g., BEAR). Noticeably, the errors on the estimate of the content of the various compounds also depend on each other, and a high error in the content of one compound is sometimes associated with a low error in the content of another one, i.e., a complementary behavior is observed. This is evident for instance in Figure 4, where the errors in the estimates of the content of acidic compounds (i.e., $SiO_2$ and $Al_2O_3$) show the mentioned complementary behavior by compensating their synergic effects (e.g., on slag basicity index).

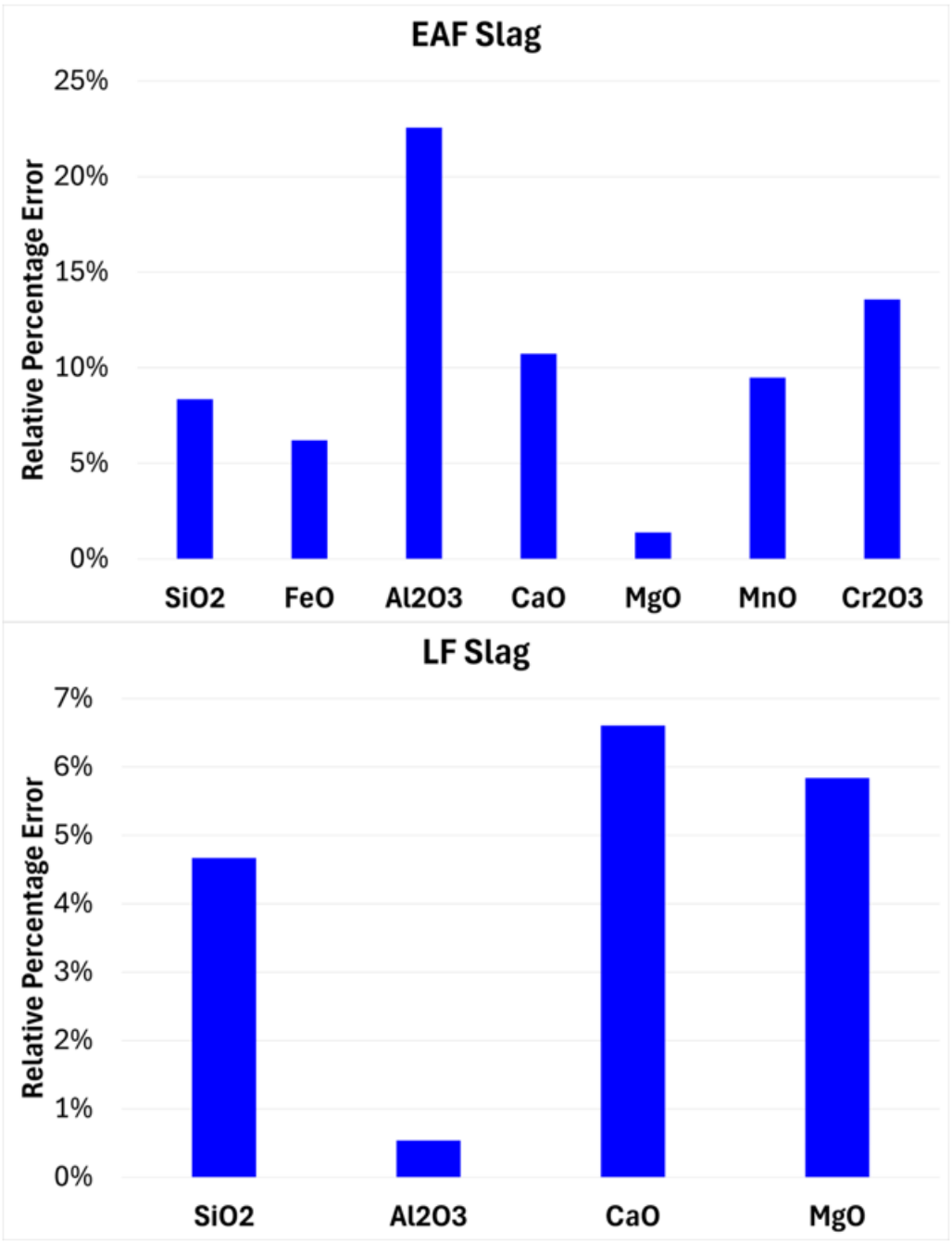


**Figure 4.** RPEs for main compounds of EAF (**top**) and LF (**bottom**) slags belonging to a single simulated heat.

The reasons of the low accuracy values in the estimates of the contents of $Al_2O_3$ and $SiO_2$ for EAF slag and of $Al_2O_3$ and MgO for LF slag are multiple. Firstly, the phenomena related to the interactions between the refractory material and the molten bath (both metal and slag) are not considered nor included in the model. Moreover, the exploited industrial data can also be affected by issues. Slag analyses can be inaccurate, for instance, because the analyzed slag sample they refer to is not representative of the analyzed slag overall. Scrap contamination negatively affects the representativeness of the used data concerning scraps, in particular as a result of tramp elements and the variability of quality and composition. Furthermore, lack of data on some variables makes it difficult to check the closure of balances: for instance, the total amount of produced LF slag is not measured on a heat basis, and only an empirical average value (4500 kg/heat) is available. However, the

model is capable of providing an estimate of slags composition for a specific heat, which is sufficient for scenario analyses assessing, for instance, the impact of variations in the operational practice or in the EAF charge mix. The suitability of the model is confirmed by the comparison between MRPE and PVC values: the MRPE trends are in line with the PCV trends in that the model shows high MRPE values for compounds whose measurements are characterized by high value of PVC.

**Table 2.** Accuracy indexes for the prediction of the contents of the main EAF slag compounds for each considered steel family and the deviation index of the related datasets.

| Steel Family | | ACH | AQT | BEAR | CCH | CQT | FC | MA | SPR |
|---|---|---|---|---|---|---|---|---|---|
| **Compound** | **Accuracy Index & Deviation Index** | | | | | | | | |
| $SiO_2$ | MRPE | 26.6% | 30.6% | 17.3% | 16.8% | 26.4% | 26.7% | 26.5% | 25.9% |
| | RMSE | 0.024 | 0.027 | 0.023 | 0.018 | 0.025 | 0.024 | 0.022 | 0.021 |
| | SI | 33.3% | 36.4% | 17.5% | 22.1% | 32.5% | 31.1% | 30.6% | 29.6% |
| | PVC | 22.9% | 20.5% | 5.1% | 9.5% | 19.8% | 21.6% | 23.7% | 22.9% |
| FeO | MRPE | 13.9% | 15.2% | 22.4% | 10.7% | 13.0% | 14.6% | 15.1% | 11.0% |
| | RMSE | 0.080 | 0.081 | 0.063 | 0.052 | 0.074 | 0.072 | 0.085 | 0.072 |
| | SI | 16.7% | 17.5% | 26.3% | 11.6% | 15.8% | 16.0% | 18.0% | 16.1% |
| | PVC | 13.9% | 13.5% | 16.2% | 10.9% | 14.6% | 13.6% | 16.8% | 11.9% |
| $Al_2O_3$ | MRPE | 38.8% | 40.3% | 15.7% | 46.0% | 30.9% | 21.7% | 38.9% | 20.5% |
| | RMSE | 0.016 | 0.017 | 0.018 | 0.022 | 0.018 | 0.014 | 0.017 | 0.013 |
| | SI | 37.6% | 39.0% | 20.9% | 40.1% | 32.0% | 22.4% | 35.4% | 26.4% |
| | PVC | 32.8% | 35.0% | 14.2% | 32.8% | 24.5% | 23.2% | 31.1% | 22.1% |
| CaO | MRPE | 17.5% | 19.3% | 6.7% | 15.9% | 18.3% | 20.8% | 19.6% | 13.8% |
| | RMSE | 0.042 | 0.051 | 0.028 | 0.028 | 0.044 | 0.046 | 0.047 | 0.033 |
| | SI | 23.6% | 24.9% | 8.2% | 15.3% | 24.6% | 22.0% | 23.0% | 16.7% |
| | PVC | 24.7% | 23.5% | 3.1% | 19.0% | 29.0% | 28.2% | 25.2% | 20.8% |
| MgO | MRPE | 14.1% | 14.6% | 10.0% | 14.4% | 12.5% | 14.6% | 13.0% | 15.3% |
| | RMSE | 0.015 | 0.013 | 0.013 | 0.012 | 0.013 | 0.013 | 0.012 | 0.012 |
| | SI | 20.3% | 18.1% | 15.0% | 14.4% | 16.9% | 17.6% | 17.0% | 17.6% |
| | PVC | 9.8% | 9.7% | 12.0% | 0.9% | 10.9% | 13.3% | 12.8% | 12.8% |
| MnO | MRPE | 11.7% | 10.5% | 12.0% | 11.0% | 12.5% | 13.7% | 12.1% | 9.1% |
| | RMSE | 0.013 | 0.012 | 0.009 | 0.011 | 0.014 | 0.013 | 0.012 | 0.010 |
| | SI | 13.8% | 13.0% | 12.0% | 12.1% | 15.7% | 14.8% | 14.6% | 11.5% |
| | PCV | 14.8% | 13.3% | 2.5% | 8.3% | 12.1% | 21.8% | 16.4% | 12.0% |
| $Cr_2O_3$ | MRPE | 24.6% | 18.2% | 22.9% | 9.4% | 13.6% | 7.5% | 17.2% | 13.4% |
| | RMSE | 0.012 | 0.009 | 0.005 | 0.003 | 0.005 | 0.003 | 0.006 | 0.006 |
| | SI | 28.3% | 23.0% | 25.3% | 10.3% | 16.9% | 9.3% | 20.7% | 17.8% |
| | PVC | 34.7% | 27.0% | 15.2% | 4.3% | 18.5% | 15.5% | 21.7% | 20.2% |

As already specified in previous sections, besides slags composition, the model also estimates other variables that are usually monitored during the evolution of the production process. Therefore, for the sake of completeness, Table 4 shows the MRPE values observed for the following relevant variables that can be computed by the model: amounts of tapped steel and liquid steel to the CC, amounts of EAF and LF slags, electrical energy required at EAF and LF and liquid steel composition in terms of mass fractions of the elements constituting more than 95% in mass of total alloy elements and other compounds other than iron. The MRPE values in Table 4 refer to the whole test dataset, thus they consider all the simulated steel families.

**Table 3.** Accuracy indexes for the prediction of the contents of the main LF slag compounds for each considered steel family and the deviation index of the related datasets.

| Steel Family | | ACH | AQT | BEAR | CCH | CQT | FC | MA | SPR |
|---|---|---|---|---|---|---|---|---|---|
| **Compound** | **Accuracy Index & Deviation Index** | | | | | | | | |
| $SiO_2$ | MRPE | 13.1% | 10.3% | 34.8% | 13.7% | 14.9% | 6.2% | 11.4% | 12.4% |
| | RMSE | 0.039 | 0.035 | 0.064 | 0.033 | 0.047 | 0.018 | 0.038 | 0.045 |
| | SI | 15.6% | 13.9% | 36.3% | 13.2% | 18.1% | 8.6% | 14.0% | 17.3% |
| | PVC | 9.3% | 10.5% | 10.3% | 18.1% | 11.1% | 6.2% | 7.0% | 10.0% |
| $Al_2O_3$ | MRPE | 29.0% | 35.4% | 7.0% | 18.6% | 59.8% | 8.9% | 24.3% | 45.7% |
| | RMSE | 0.020 | 0.024 | 0.010 | 0.009 | 0.035 | 0.009 | 0.016 | 0.027 |
| | SI | 36.9% | 38.6% | 7.5% | 18.2% | 62.0% | 10.6% | 32.7% | 51.4% |
| | PVC | 31.2% | 30.1% | 4.5% | 16.1% | 36.0% | 10.7% | 23.6% | 33.1% |
| CaO | MRPE | 7.6% | 4.6% | 19.0% | 8.6% | 4.9% | 1.9% | 3.9% | 5.8% |
| | RMSE | 0.056 | 0.040 | 0.122 | 0.063 | 0.038 | 0.016 | 0.030 | 0.048 |
| | SI | 8.9% | 6.3% | 19.2% | 10.1% | 6.1% | 2.4% | 4.8% | 7.8% |
| | PVC | 3.6% | 4.7% | 3.2% | 1.2% | 5.6% | 2.3% | 3.3% | 5.4% |
| MgO | MRPE | 24.2% | 39.3% | 13.6% | 15.9% | 42.9% | 12.9% | 25.7% | 66.6% |
| | RMSE | 0.015 | 0.028 | 0.007 | 0.005 | 0.029 | 0.007 | 0.058 | 0.037 |
| | SI | 35.1% | 61.6% | 16.6% | 15.0% | 56.3% | 15.8% | 34.5% | 60.9% |
| | PVC | 32.1% | 58.1% | 14.0% | 20.0% | 54.5% | 13.8% | 35.6% | 57.4% |

Table 4 shows how the model provides accurate estimates of the listed variables; the accuracy values observed in the estimates of the required electrical energy and of the amount and composition of liquid steel are noticeably high, and only the estimate of the content of V in steel shows an error higher than 15%; nevertheless, the absolute value of this variable content is very low. The higher error in the estimates of slag amounts with respect to steel amount can be explained by the strict correlation between the two variables; since a higher amount of steel compared to slag is produced, a lower error in the prediction of the steel amount results in a higher error in slag amount estimate. Nevertheless, some of these errors are related to the lack of regular monitoring of some variables; this problem affects the feasibility of checking the closure of balances and consequently affects the model's accuracy. This consideration is valid, for instance, for the amount of LF slag, as well as for the amount and composition of off-gases and dusts. However, the good accuracy in the estimates of steel amount and composition shows that the errors in slag characterization do not negatively affect the overall representation of the process and steel production provided by the model due to the previously mentioned complementarity of these errors, which mutually compensate their effects on the estimate of important slag features (e.g., basicity) affecting steel composition. This fact further shows that, despite issues in the original industrial data, the model provides outcomes that can help in finding where industrial data lack reliability, as it is based on physical/chemical laws and not only on empirical correlations.

**Table 4.** MRPEs of some of the variables that can be computed with the electric steelmaking route flowsheet model.

| Variable | MRPE |
|---|---|
| Amount of Tapped Steel | 4.5% |
| Amount of Liquid Steel to CC | 3.4% |
| Amount of EAF Slag | 26.8% |
| Amount of LF Slag * | 9.7% |
| EAF Electrical Energy | 0.3% |
| LF Electrical Energy | 0.5% |

**Table 4.** *Cont.*

| Variable | MRPE |
|---|---|
| C content ($w/w$) in Liquid Steel to CC | 6.1% |
| Mn content ($w/w$) in Liquid Steel to CC | 2.4% |
| Si content ($w/w$) in Liquid Steel to CC | 1.3% |
| Cr content ($w/w$) in Liquid Steel to CC | 11.2% |
| Ni content ($w/w$) in Liquid Steel to CC | 5.8% |
| Mo content ($w/w$) in Liquid Steel to CC | 2.3% |
| V content ($w/w$) in Liquid Steel to CC | 24.1% |
| Cu content ($w/w$) in Liquid Steel to CC | 0.6% |

* for LF slag amount, no heat-based industrial data were available; only an empirical average value of 4500 kg/heat was given.

## 4. Discussion

The obtained results show that the upgraded model can provide suitable indications of the expected compositions of slags on a heat basis by supporting the optimal management, handling and valorization of slags. Furthermore, the model can be the basis for more complex tools that can be developed for real-time decision making focused on improving slag composition, e.g., to optimize the logistics (e.g., to avoid mixing slags with completely different features) and improve reuse and/or recycling potential.

In addition, the potential to monitor several aspects of process, product and by-products throughout the whole electric steelmaking cycle enables scenario analyses, e.g., investigations of conventional and unconventional operating practices, conditions, configurations or processes carried out by assessing the joint effects on steel, slags and overall energy performance of the production process. Thus, the presented model overcomes the limits of available models from the literature [29] that are focused on one type of slag or on specific areas/steps of the production process. In addition, the model's feature to be easily customized with standard data makes it easily transferable, and its modularity also allows customization in case of new process steps, new operating conditions or new feedstocks, overcoming another limitation of very complex models in the literature [30–34].

Furthermore, the model accuracy, although for some aspects suitable only for semi-quantitative investigations, can still be improved. This confirms what is already highlighted in the literature related to issues of data quality and reliability [28]. Although more information that can be used for model upgrading is collected now compared to the past and although most involved phenomena are theoretically known, some specific empirical/hidden process behaviors characterizing the industrial process are strictly affected by the variability of feedstocks (i.e., scrap in this case). These behaviors can be better captured having more reliable data related to feedstocks and variables that are currently discontinuously monitored (e.g., fumes, amount of LF slags), refining the "steel families", or using novel devices and protocols to provide more representative analyses of slag composition. Slags are indeed a very heterogeneous material, and a single sample might not be representative, but slag analyses are costly and time-consuming. Devices allowing fast multiple sampling and analyses can improve the quality of gathered information, and higher model performances can be achieved thanks to greater consistency in the data. Specific data-collection campaigns can also be carried out to gather information on unmodelled phenomena (e.g., interaction between refractory material and the molten bath) to further improve its performance. Furthermore, when high-quality data are available, the flowsheet model can be improved by hybridizing it, using data-driven techniques to capture "hidden" and unmodelled phenomena by discovering correlations within the data.

## 5. Conclusions

Knowing the composition of by-products of industrial processes can support the improvement of material efficiency, along with the extensive application of circular economy approaches and industrial symbiosis. This is the case for slags produced in the electric steelmaking route. Although slags are recognized as valuable sources of secondary raw materials, their reuse, recycling and valorization in general are not optimized because their composition is often not continuously monitored, and variations due to alterations in standard operating practices cannot be estimated. Therefore, in the paper, a stationary flowsheet model was presented to estimate EAF and LF slags compositions on a heat basis; this model also allows the computation of other standard monitored process variables. The model accuracy is generally sufficient to provide indications on the content of main components of the slag. Indeed, for more than 70% of tested heats, RPE values lower than 25% were obtained for FeO, CaO, MgO, MnO and $Cr_2O_3$ in EAF slag and for $SiO_2$ and CaO in LF slag; furthermore, the model performance is aligned with the PVC values of the compounds. For other compounds (i.e., $SiO_2$ and $Al_2O_3$ in EAF slags and $Al_2O_3$ and MgO in LF slags), only semi-quantitative results are provided and accuracy is still limited, although the order of magnitudes is respected. Further improvements will be achievable when more reliable data are provided, for instance, by novel sensing devices and novel protocols for slag and scrap analyses.

Nevertheless, the presented model can be considered a valuable and transferable tool with which to obtain indications on EAF and LF slags composition, to drive decision-making on slag valorization with or without conditioning steps and/or to explore the effects of process modifications on the composition of slags and steel, as well as on other relevant process variables. The model can be used to evaluate solutions to jointly improve steel and slag qualities and process sustainability.

Finally, besides its usefulness for scenario analyses, the presented model is currently used as the basis of a hybrid model (merging machine learning and physics-based modelling approaches) characterized by a lower computational burden, which can be used in a real-time decision-support system to provide indications on the most suitable pathways for slags valorization. Further developments are ongoing to extend the model to consider the effects of hydrogen-reduced hot briquetted iron (HBI) and/or DRI.

**Author Contributions:** Conceptualization, I.M. and V.C.; methodology, I.M.; software, I.M., A.P. and A.Z.; validation, I.M., A.P. and A.Z.; formal analysis, I.M. and V.C.; investigation, I.M., A.P., V.C. and A.Z.; resources, V.C.; data curation, M.F.P., R.A.P., A.P., A.Z. and I.M.; writing—original draft preparation, I.M.; writing—review and editing, V.C., M.F.P. and R.A.P.; visualization, A.P., A.Z. and R.A.P.; supervision, V.C.; project administration, V.C.; funding acquisition, V.C. All authors have read and agreed to the published version of the manuscript.

**Funding:** This research was funded by the European Union through the Research Fund for Coal and Steel (RFCS), Grant Agreement No 899164.

**Data Availability Statement:** The original contributions presented in this study are included in the article. Further requests can be directed to the corresponding author.

**Acknowledgments:** The work described in the present paper was developed within the project entitled "Optimising slag reuse and recycling in electric steelmaking at optimum metallurgical performance through on-line characterization devices and intelligent decision support system" (iSlag-G.A. 899164) co-funded by the Research Fund for Coal and Steel of the European Union, which is gratefully acknowledged. The sole responsibility of the issues treated in the present paper lies with the authors; the Union is not responsible for any use that may be made of the information contained therein.

**Conflicts of Interest:** Authors Maria Prieto Ferrer and Raquel Pérez Arias were employed by the company Sidenor Investigacion Y Desarrollosa. The remaining authors declare that the research was conducted in the absence of any commercial or financial relationships that could be construed as a potential conflict of interest.

## References


1. European Commission. The European Green Deal—Striving to Be the First Climate-Neutral Continent. Available online: https://commission.europa.eu/strategy-and-policy/priorities-2019-2024/european-green-deal_en (accessed on 22 November 2024).
2. European Commission. Circular Economy Action Plan—The EU's New Circular Action Plan Paves the Way for a Cleaner and More Competitive Europe. Available online: https://environment.ec.europa.eu/strategy/circular-economy-action-plan_en (accessed on 22 November 2024).
3. ESTEP. Improve the EAF Scrap Route for a Sustainable Value Chain in the EU Circular Economy Scenario–ROADMAP—An Evolution Document for a Strategic Look to the Future of European EAF Steelmaking. Available online: https://www.estep.eu/assets/Publications/Improve-the-EAF-scrap-route-Roadmap-Final-V2-3.pdf (accessed on 8 November 2024).
4. Rodríguez Diez, J.; Tomé-Torquemada, S.; Vicente, A.; Reyes, J.; Orcajo, G.A. Decarbonization Pathways, Strategies, and Use Cases to Achieve Net-Zero $CO_2$ Emissions in the Steelmaking Industry. *Energies* **2023**, *16*, 7360. [CrossRef]
5. Kazmi, B.; Taqvi, S.A.A.; Juchelková, D. State-of-the-art review on the steel decarbonization technologies based on process system engineering perspective. *Fuel* **2023**, *347*, 128459. [CrossRef]
6. Conde, A.S.; Rechberger, K.; Spanlang, A.; Wolfmeir, H.; Harris, C. Decarbonization of the steel industry. A techno-economic analysis. *Matér. Tech.* **2021**, *109*, 305. [CrossRef]
7. Dettori, S.; Matino, I.; Colla, V.; Speets, R. A Deep Learning-based approach for forecasting off-gas production and consumption in the blast furnace. *Neural Comput. Appl.* **2022**, *34*, 911–923. [CrossRef]
8. Na, H.; Yuan, Y.; Sun, J.; Zhang, L.; Du, T. Integrative optimization for energy efficiency, $CO_2$ reduction, and economic gains in the iron and steel industry: A holistic approach. *Resour. Conserv. Recycl.* **2025**, *212*, 107992. [CrossRef]
9. Dettori, S.; Matino, I.; Colla, V.; Weber, V.; Salame, S. Neural network-based modeling methodologies for energy transformation equipment in integrated steelworks processes. *Energy Procedia* **2019**, *158*, 4061–4066. [CrossRef]
10. Porzio, G.F.; Colla, V.; Fornai, B.; Vannucci, M.; Larsson, M.; Stripple, H. Process integration analysis and some economic-environmental implications for an innovative environmentally friendly recovery and pre-treatment of steel scrap. *Appl. Energy* **2016**, *161*, 656–672. [CrossRef]
11. Mapelli, C.; Dall'Osto, G.; Mombelli, D.; Barella, S.; Gruttadauria, A. Future scenarios for reducing emissions and consumption in the Italian steelmaking industry. *Steel Res. Int.* **2022**, *93*, 2100631. [CrossRef]
12. Echterhof, T. Review on the use of alternative carbon sources in EAF steelmaking. *Metals* **2021**, *11*, 222. [CrossRef]
13. Di Giovanni, C.; Echterhof, T. Progress Toward Biocarbon Utilization in Electric Arc Furnace Steelmaking: Current Status and Future Prospects. *J. Sustain. Metall.* **2024**, *10*, 2047–2067. [CrossRef]
14. Henriques, J.; Castro, P.M.; Dias, R.; Magalhães, B.; Estrela, M. Potential Industrial Synergies in the Steelmaking and Metal-Processing Industry: By-Products Valorization and Associated Technological Processes. *Sustainability* **2023**, *15*, 15323. [CrossRef]
15. Matino, I.; Branca, T.A.; Fornai, B.; Colla, V.; Romaniello, L. Scenario Analyses for By-Products Reuse in Integrated Steelmaking Plants by Combining Process Modeling, Simulation, and Optimization Techniques. *Steel Res. Int.* **2019**, *90*, 1900150. [CrossRef]
16. Branca, T.A.; Fornai, B.; Colla, V.; Pistelli, M.I.; Faraci, E.L.; Cirilli, F.; Schröder, A.J. Industrial symbiosis and energy efficiency in european process industries: A review. *Sustainability* **2021**, *13*, 9159. [CrossRef]
17. Worldsteel Association. Fact Sheet-Steel Industry Co-Products. Available online: https://worldsteel.org/wp-content/uploads/Fact-sheet-Steel-industry-co-products.pdf (accessed on 15 November 2024).
18. Worldsteel Association. Public Policy Paper—Steel Industry Co-Products. Available online: https://worldsteel.org/publications/bookshop/steel-industry-co-products-ppp/ (accessed on 15 November 2024).
19. Das, P.; Upadhyay, S.; Dubey, S.; Singh, K.K. Waste to wealth: Recovery of value-added products from steel slag. *J. Environ. Chem. Eng.* **2021**, *9*, 105640. [CrossRef]
20. Ye, G.; Burström, E.; Kuhn, M.; Piret, J. Reduction of steel-making slags for recovery of valuable metals and oxide materials. *Scand. J. Metall.* **2003**, *32*, 7–14. [CrossRef]
21. Motz, H.; Geiseler, J. Products of steel slags an opportunity to save natural resources. *Waste Manag.* **2001**, *21*, 285–293. [CrossRef]
22. Branca, T.A.; Colla, V.; Valentini, R. A way to reduce environmental impact of ladle furnace slag. *Ironmak. Steelmak.* **2009**, *36*, 597–602. [CrossRef]
23. Herbelin, M.; Bascou, J.; Lavastre, V.; Guillaume, D.; Benbakkar, M.; Peuble, S.; Baron, J.P. Steel slag characterisation—Benefit of coupling chemical, mineralogical and magnetic techniques. *Minerals* **2020**, *10*, 705. [CrossRef]
24. Menad, N.E.; Kana, N.; Seron, A.; Kanari, N. New eaf slag characterization methodology for strategic metal recovery. *Materials* **2021**, *14*, 1513. [CrossRef]

25. Petersson, J.; Gilbert-Gatty, M.; Bengtson, A. Rapid chemical analysis of steel slag by laser-induced breakdown spectroscopy for near-the-line applications. *J. Anal. At. Spectrom.* **2020**, *35*, 1848–1858. [CrossRef]
26. Dong, C.; Yu, H.; Sun, L.; Li, Y.; Liu, X.; Zhou, P.; Huang, S. Characteristics of laser-induced breakdown spectroscopy of liquid slag. *Plasma Sci. Technol.* **2024**, *26*, 025502. [CrossRef]
27. Long, S.; Li, M.-G.; Chou, J.-J.; Zhang, T.L.; Tang, H.-S.; Li, H. Rapid quantitative analysis of slag acidity by laser induced breakdown spectroscopy combined with random forest. *Chin. J. Anal. Chem.* **2023**, *51*, 100210. [CrossRef]
28. Murua, M.; Boto, F.; Anglada, E.; Cabero, J.M.; Fernandez, L. A slag prediction model in an electric arc furnace process for special steel production. *Procedia Manuf.* **2021**, *54*, 178–183. [CrossRef]
29. Hay, T.; Reimann, A.; Echterhof, T. Improving the Modeling of Slag and Steel Bath Chemistry in an Electric Arc Furnace Process Model. *Metall. Mater. Trans. B* **2019**, *50*, 2377–2388. [CrossRef]
30. Fathi, A.; Saboohi, Y.; Škrjanc, I.; Logar, V. Comprehensive Electric Arc Furnace Model for Simulation Purposes and Model-Based Control. *Steel Res. Int.* **2017**, *88*, 1600083. [CrossRef]
31. Logar, V.; Dovžan, D.; Škrjanc, I. Modeling and validation of an electric arc furnace: Part 1, heat and mass transfer. *ISIJ Int.* **2012**, *52*, 402–412. [CrossRef]
32. Logar, V.; Dovžan, D.; Škrjanc, I. Modeling and validation of an electric arc furnace: Part 2, thermo-chemistry. *ISIJ Int.* **2012**, *52*, 413–423. [CrossRef]
33. Harada, A.; Maruoka, N.; Shibata, H.; Kitamura, S.Y. A kinetic model to predict the compositions of metal, slag and inclusions during ladle refining: Part 1. Basic concept and application. *ISIJ Int.* **2013**, *53*, 2110–2117. [CrossRef]
34. Harada, A.; Maruoka, N.; Shibata, H.; Kitamura, S.Y. A kinetic model to predict the compositions of metal, slag and inclusions during ladle refining: Part2. Condition to control the inclusion composition. *ISIJ Int.* **2013**, *53*, 2118–2125. [CrossRef]
35. Publications Office of the European Union. Final Report of GA: RFSR-CT-2013-00030. Environmental Impact Evaluation and Effective Management of Resources in the EAF Steelmaking–EIRES. Available online: https://op.europa.eu/en/publication-detail/-/publication/b9552f10-5a49-11e8-ab41-01aa75ed71a1 (accessed on 1 December 2024).
36. Matino, I.; Alcamisi, E.; Colla, V.; Baragiola, S.; Moni, P. Process modelling and simulation of electric arc furnace steelmaking to allow prognostic evaluations of process environmental and energy impacts. *Matér. Tech.* **2016**, *104*, 104. [CrossRef]
37. Colla, V.; Matino, I.; Cirilli, F.; Jochler, G.; Kleimt, B.; Rosemann, H.; Unamuno, I.; Tosato, S.; Gussago, F.; Baragiola, S.; et al. Improving energy and resource efficiency of electric steelmaking through simulation tools and process data analyses. *Matér. Tech.* **2016**, *104*, 602. [CrossRef]
38. Matino, I.; Colla, V.; Baragiola, S. Internal slags reuse in an electric steelmaking route and process sustainability: Simulation of different scenarios through the EIRES monitoring tool. *Waste Biomass Valorization* **2018**, *9*, 2481–2491. [CrossRef]
39. Heo, J.H.; Park, J.H. Effect of Slag Composition on Dephosphorization and Foamability in the Electric Arc Furnace Steelmaking Process: Improvement of Plant Operation. *Metall. Mater. Trans. B* **2021**, *52*, 3613–3623. [CrossRef]
40. Violi, G. *Processi Siderurgici—La Fabbricazione Della Ghisa e Dell'acciaio*; ETAS KOMPASS: Milano, Italy, 1972.
41. Nicodemi, W.; Mapelli, C. *Siderurgia*; AIM: Milano, Italy, 2011.
42. Baghforth, R.G. *The Manufacture of Iron and Steel Vol. II*; Creative Media Partners, LLC: London, UK, 2017.